Available online at www.sciencedirect.com

ScienceDirect

Mendeleev Commun., 2020, **30**, 583–585

Mendeleev Communications

Discrimination of enzyme–substrate complexes by reactivity using the electron density analysis: peptide bond hydrolysis by the matrix metalloproteinase-2

Maria G. Khrenova,*[a,b] Alexander V. Nemukhin[b,c] and Vladimir G. Tsirelson[d]

[a] *A. N. Bach Institute of Biochemistry, Federal Research Centre 'Fundamentals of Biotechnology', Russian Academy of Sciences, 119071 Moscow, Russian Federation. E-mail: khrenova.maria@gmail.com*
[b] *Department of Chemistry, M. V. Lomonosov Moscow State University, 119991 Moscow, Russian Federation*
[c] *N. M. Emanuel Institute of Biochemical Physics, Russian Academy of Sciences, 119334 Moscow, Russian Federation*
[d] *D. I. Mendeleev University of Chemical Technology of Russia, 125047 Moscow, Russian Federation*

DOI: 10.1016/j.mencom.2020.09.010

The results of quantum mechanics/molecular mechanics calculations of electron density changes upon oligopeptide hydrolysis by the matrix metalloproteinase-2 are utilized to discriminate between reactive and non-reactive enzyme–substrate complexes. Electron density depletion regions on the carbonyl carbon atom attacked by a catalytic water molecule are found on the 2D maps of electron density Laplacian in the reactive complexes. Also, the computed Fukui function quantitatively describes reactivity of the nucleophilic and electrophilic sites.

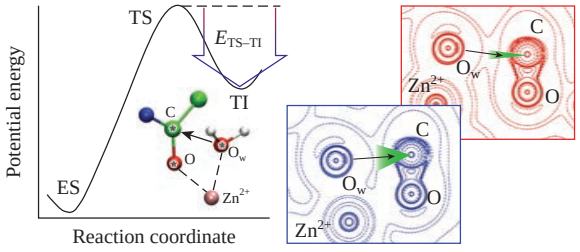

Keywords: metalloenzymes, matrix metalloproteinase-2, QM/MM, Laplacian of electron density, reactivity, nucleophilic addition.

A peptide bond is inert in aqueous solutions and hydrolyzes with a half-life of centuries.[1] However, upon binding to a protease active site reaction rate constants increase to tens or even hundreds of reciprocal seconds.[2] Main reasons of such enormous hydrolysis acceleration are carbonyl group activation and shortening the nucleophilic attack distance in enzyme–substrate complexes. Depending on a particular protease, activation of the carbonyl bond occurs differently. Many enzymes include a fragment called an oxyanion hole that polarizes the >C=O fragment and stabilizes the forming negatively charged tetrahedral intermediate by hydrogen bonds.[3] In case of metalloenzymes,[2] the carbonyl group forms a weak coordination interaction with a metal cation that strengthens upon the formation of reaction intermediates. The short distance of nucleophilic attack is supported by the tight spatial organization of enzyme active site.

In this work, we focus on the matrix metalloproteinase-2 (MMP-2), a zinc-dependent endopeptidase responsible for peptide bond cleavage in the extracellular matrix. As shown previously,[4–6] the quantum mechanics/molecular mechanics (QM/MM) method is a proper tool to characterize reaction mechanism in this zinc-dependent enzyme. The first step in the hydrolysis reaction is a nucleophilic attack of a Zn^{2+}-coordinated water molecule on the peptide carbonyl group. It starts from an enzyme–substrate complex (ES) and leads to the formation of a tetrahedral intermediate (TI) (Scheme 1).

Benchmark studies[6] showed that not every equilibrium molecular structure of an enzyme–substrate (ES) complex corresponds to a reactive state. More specifically, not every potential energy profile initiated from one of these ES complexes, *i.e.*, from one of the competing minima on the potential energy surface, could reach a minimum energy point corresponding to a tetrahedral intermediate. Each profile can be quantified by the stabilization energy of TI relative to the corresponding transition state (TS) as shown in Figure 1. This observation is in line with the idea of the equilibrium between the reactive (ES^R) and non-reactive (ES^N) populations of the enzyme–substrate complexes.[7,8] The ES^R initiates a productive potential energy profile of the chemical reaction, and ES^N corresponds to a non-productive one. The attempts to discriminate ES complexes by their reactivity using selected sets of ES geometry parameters were not successful.[6] Apparently, their reactivity appears as a balance of multiple contributions.

Herein we suggest to apply electron density analysis to a set of ES complexes of a model system composed of MMP-2 and an oligopeptide substrate[6] to classify them as reactive or non-

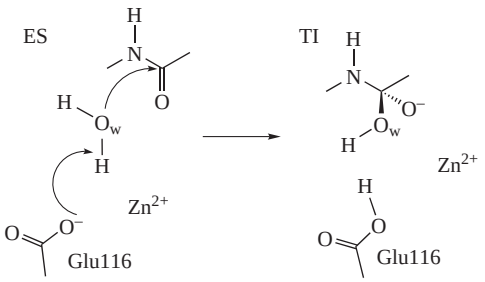

Scheme 1 Nucleophilic attack mechanism on the substrate carbonyl carbon atom in active site of MMP-2.

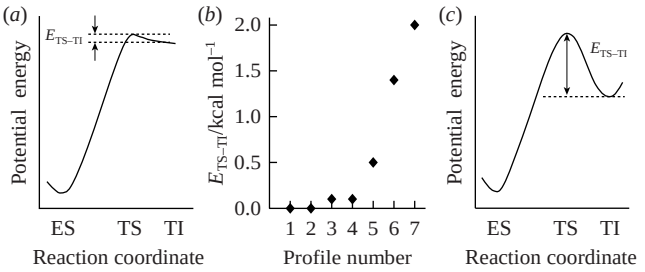

Figure 1 Left and right panels illustrate potential energy profiles of the first step of the peptide bond hydrolysis reaction in the active site of MMP-2 showing (*a*) non-productive and (*c*) productive cases. The E_{TS-TI} values shown in the central panel (*b*) refer to the stabilization energy of TI relative to TS as computed for seven different profiles in ref. 6. Profiles 1–4 are non-productive, 5 is intermediate and 6–7 are productive.

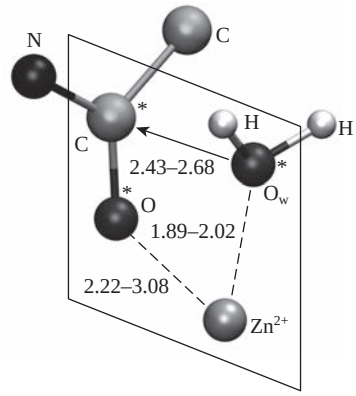

Figure 2 Molecular model of the ES complex fragment involved in the reaction. The arrow depicts direction of the nucleophilic attack on substrate carbonyl group; dashed lines correspond to coordination interactions with Zn^{2+}. Ranges of interatomic distances in profiles 1–7 are given in Å. Atoms marked with asterisks form a plane for the electron density Laplacian calculations shown in Figure 3.

reactive.† We utilized the Fukui function that categorizes sites for nucleophilic and electrophilic attack and analyzed electron density Laplacian to establish differences between two groups of energy profiles.

The available data on seven potential energy profiles of the first step of oligopeptide hydrolysis in the active site of MMP-2[6] allows one to classify them by TI stabilization energy relative to the transition state TS [Figure 1(*b*)]. The TI in profiles 6 and 7 is more than 1 kcal mol^{-1} stable relative to the corresponding TS. Therefore, we suppose that ESs from these profiles are reactive. Profile 5 is characterized by a smaller stabilization energy (0.5 kcal mol^{-1}) and it holds an intermediate position. The tetrahedral intermediates in profiles 3 and 4 have almost the same energy as the corresponding TSs. This means that such TIs decay back to the ES as only they are formed. Minima in profiles 1 and 2 corresponding to the tetrahedral intermediates are not located. Thus, profiles 6 and 7 are productive, the profile 5 is intermediate and profiles 1–4 are non-productive.

Key interatomic distances that can determine ES reactivity are the distance of nucleophilic attack C–O_w, and two coordination interaction distances, Zn^{2+}–O_w and Zn^{2+}–O (Figure 2). Only Zn^{2+}–O_w distance gradually changes according to productivity attributed to each profile. However, variation of this parameter is very small and does not exceed 0.15 Å and it can hardly be utilized to classify the ES complexes.

We analyzed electron density features of ES and TI states for seven available potential energy profiles[6] to better understand the determinant of their different productivity. It is known that electron density Laplacian reveals the areas of electron concentration [$\nabla^2\rho(r) < 0$] and depletion [$\nabla^2\rho(r) > 0$] and can be utilized for activated double bond reactivity prediction.[9–13] It is also applied to characterize tetrel bonds in molecular complexes which are of the same nature as interatomic interactions discussed previously.[14,15] The Laplacian of electron density in the O=C–O_w plane (see Figure 2) is presented in Figure 3. The differences between reactive (ES^R) and nonreactive (ES^N) complexes and corresponding tetrahedral intermediates are the following. In ES^R, the electron depletion area on the carbon atom at the side of nucleophilic attack is larger than that in ES^N. The corresponding quantitative estimate may be taken as the diameter of the electron-density hole limited by $\nabla^2\rho = 0$ isolines in the plane under consideration. It is higher than 0.3 Å for ES^R and lower than 0.2 Å in ES^N. The electron density features of the newly formed C–O_w covalent bond are also different. In case of stabilized intermediate (TI^R) we observe a remarkable area of $\nabla^2\rho < 0$, indicating formation of a stable covalent bond. By contrast, the electron density concentration region along C–O_w direction is narrow in non-stabilized

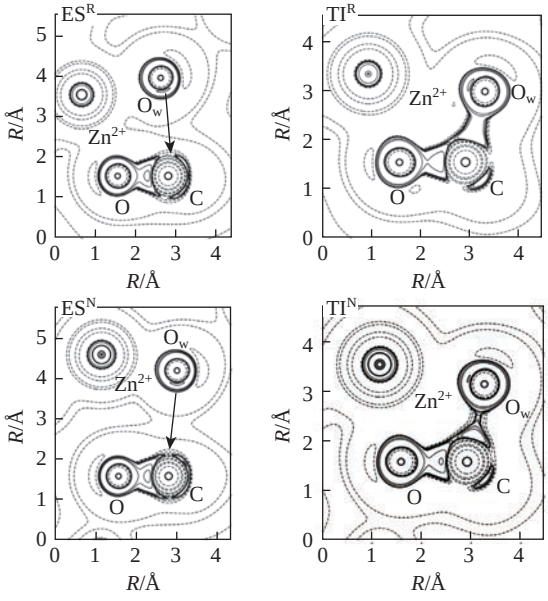

Figure 3 Electron density Laplacian $\nabla^2\rho(r)$ in the plane of O_w, C and O atoms. Reactive ES and TI states (ES^R and TI^R) are shown in the upper row, non-reactive ES and TI states (ES^N and TI^N) are shown in the lower row. The contour lines for $\nabla^2\rho(r)$ are $\pm(1, 5)\times10^n$ a.u., $-1 \leqslant n \leqslant 1$. Dashed contour lines indicate the electron density depletion areas and solid lines identify the electron density concentrations. The arrow points to the direction of nucleophilic attack.

† *Computational protocol*. The equilibrium geometry configurations obtained with the quantum mechanics/molecular mechanics (QM/MM) method, QM(PBE0-D3/6-31G**)/MM(CHARMM), in ref. 6 were utilized for the electron density analysis. Those correspond to seven potential energy profiles.[6] Electron densities of a set of QM subsystems of seven ES and TI complexes were calculated at the PBE0-D3/6-31G** level of theory using the Firefly quantum chemistry package[17] partially based on the GAMESS (US)[18] source code. The 2D maps of electron density Laplacian were calculated in the plane of atoms O_w, C and O. The values of Fukui function[16] were estimated for the O_w and C atoms as an average value on a local molecular surface corresponding to a selected atom. The molecular surface was determined at the isovalue of ρ = 0.01 a.u. Fukui functions for the sites of nucleophilic (f^+) and electrophilic (f^-) attack were calculated according to the formulae: $f^+(r) = \rho_{N+1}(r) - \rho_N(r)$, $f^-(r) = \rho_N(r) - \rho_{N-1}(r)$, where $\rho_N(r)$ is the electron density of an N-electron ES system under consideration. The $\rho_{N+1}(r)$ and $\rho_{N-1}(r)$ electron densities were calculated at the same geometry configuration by adding or withdrawing an electron and changing electronic state from singlet to doublet. Electron density features were calculated using Multiwfn program,[19] equilibrium geometry configurations were visualized in the VMD package.[20]

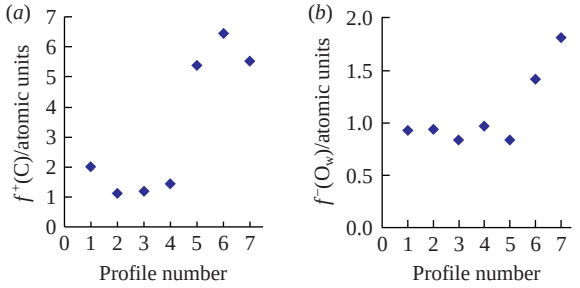

Figure 4 Fukui functions, (*a*) f^+(C) and (*b*) f^-(O_w) calculated for a set of seven ES complexes considered in ref. 6.

TI^N as the covalent bond is unstable and can easily be broken, returning the system back to the ES^N state.

We also used the Fukui functions f^+ and f^- to predict reactivity of nucleophilic and electrophilic sites, respectively,[16] and to quantify the reactivity of sites for nucleophilic (C) and electrophilic (O_w) attack in the ES complexes (Figure 4). The ES complexes in profiles 1–4 are non-reactive from both f^+ and f^- analyses. Profile 5 is assigned to the intermediate case by the stabilization energy $E_{TS\text{-}TI}$. The f^+(C) function has the value similar to those for reactive ES from profiles 6 and 7, indicating that carbonyl atom is activated. The f^-(O_w) function of profile 5 ES shows the same value as the non-reactive ES complexes. Thus, the origin of the intermediate nature of profile 5 ES is that the carbon atom is activated and the oxygen atom O_w is not. Both C and O_w atoms are activated in reactive ES species from profiles 6 and 7, forcing the first stage to proceed with considerable TI stabilization.

In conclusion, we demonstrate electron-density features of ES complexes that can be used to classify them to reactive and non-reactive. Electron density Laplacian indicates that electron depletion area near the carbonyl carbon atom increases at the side of nucleophilic attack in reactive species. The newly formed C–O_w covalent bond is more pronounced in stabilized intermediates, *i.e.*, the electron concentration region is wider. The Fukui function discriminates the reactive ES complexes by determination of reactivity sites for nucleophilic and electrophilic attack. Importantly, these conclusions are obtained for the complex referring to a highly polarized system that includes doubly charged metal cation participating in the chemical reaction.

MGK thanks Russian Foundation for Basic Research (project no. 18-29-13006) for the support of this study. The research is carried out using the equipment of the shared research facilities of HPC computing resources at M. V. Lomonosov Moscow State University. We also acknowledge the use of supercomputer resources of the Joint Supercomputer Center of the Russian Academy of Sciences.

Online Supplementary Materials

Supplementary data associated with this article can be found in the online version at doi: 10.1016/j.mencom.2020.09.010.

References

1 A. Radzicka and R. Wolfenden, *J. Am. Chem. Soc.*, 1996, **118**, 6105.
2 *Handbook of Proteolytic Enzymes*, 3rd edn., eds. N. D. Rawlings and G. Salvesen, Academic Press, 2013.
3 T. Klein, U. Eckhard, A. Dufour, N. Solis and C. M. Overall, *Chem. Rev.*, 2018, **118**, 1137.
4 T. Vasilevskaya, M. G. Khrenova, A. V. Nemukhin and W. Thiel, *J. Comput. Chem.*, 2015, **36**, 1621.
5 T. Vasilevskaya, M. G. Khrenova, A. V. Nemukhin and W. Thiel, *Mendeleev Commun.*, 2016, **26**, 209.
6 T. Vasilevskaya, M. G. Khrenova, A. V. Nemukhin and W. Thiel, *J. Comput. Chem.*, 2016, **37**, 1801.
7 N. Kanaan, M. Roca, I. Tuñón, S. Martí and V. Moliner, *Phys. Chem. Chem. Phys.*, 2010, **12**, 11657.
8 S. Martí, M. Roca, J. Andrés, V. Moliner, E. Silla, I. Tuñón and J. Bertrán, *Chem. Soc. Rev.*, 2004, **33**, 98.
9 M. G. Khrenova, A. M. Kulakova and A. V. Nemukhin, *Org. Biomol. Chem.*, 2020, **18**, 3069.
10 M. T. Carroll, J. R. Cheeseman, R. Osman and H. Weinstein, *J. Phys. Chem.*, 1989, **93**, 5120.
11 Z. Shi and R. J. Boyd, *J. Am. Chem. Soc.*, 1993, **115**, 9614.
12 V. G. Tsirelson, A. V. Shishkina, A. I. Stash and S. Parsons, *Acta Crystallogr.*, 2009, **B65**, 647.
13 M. G. Khrenova and V. G. Tsirelson, *Mendeleev Commun.*, 2019, **29**, 492.
14 E. Bartashevich, Y. Matveychuk and V. Tsirelson, *Molecules*, 2019, **24**, 1083.
15 P. R. Varadwaj, A. Varadwaj and B.-Y. Jin, *Phys. Chem. Chem. Phys.*, 2014, **16**, 17238.
16 R. G. Parr and W. Yang, *J. Am. Chem. Soc.*, 1984, **106**, 4049.
17 A. A. Granovsky, *Fairfly*, http://classic.chem.msu.su/gran/firefly/index.html.
18 M. W. Schmidt, K. K. Baldridge, J. A. Boatz, S. T. Elbert, M. S. Gordon, J. H. Jensen, S. Koseki, N. Matsunaga, K. A. Nguyen, S. Su, T. L. Windus, M. Dupuis and J. A. Montgomery, *J. Comput. Chem.*, 1993, **14**, 1347.
19 T. Lu and F. Chen, *J. Comput. Chem.*, 2012, **33**, 580.
20 W. Humphrey, A. Dalke and K. Schulten, *J. Mol. Graph.*, 1996, **14**, 33.

Received: 20th April 2020; Com. 20/6200